EPJ Web of Conferences **303**, 01012 (2024) https://doi.org/10.1051/epjconf/202430301012
MENU 2023

Exploring Light Meson Resonances in Two-Pion Photoproduction: A Regge Formalism Analysis

Łukasz Bibrzycki[1], *Nadine* Hammoud[2,*], *Vincent* Mathieu[3,4], *Robert J.* Perry[3], and *Adam P.* Szczepaniak[5,6,7]

[1]AGH University of Science and Technology, Faculty of Physics and Applied Computer Science, al. Mickiewicza 30, PL-30059 Kraków, Poland
[2]Institute of Nuclear Physics, Polish Academy of Sciences, 31-342 Kraków, Poland
[3]Departament de Física Quàntica i Astrofísica and Institut de Ciències del Cosmos, Universitat de Barcelona, E-08028, Spain.
[4]Departamento de Física Teórica, Universidad Complutense de Madrid and IPARCOS, E-28040 Madrid, Spain
[5]Theory Center, Thomas Jefferson National Accelerator Facility, Newport News, VA 23606, USA
[6]Center for Exploration of Energy and Matter, Indiana University, Bloomington, IN 47403, USA
[7]Department of Physics, Indiana University, Bloomington, IN 47405, USA

Abstract. In the domain of hadron spectroscopy, the investigation of meson resonances plays a pivotal role. This study focuses on the significance of two-pion photoproduction as a prominent avenue for studying meson resonances in the $\pi\pi$ system. By employing the Regge formalism, our model incorporates the background contribution from the well-known "Deck Mechanism" and emphasizes the significant $\rho(770)$ resonance, representing the P-wave contribution arising from pomeron and f_2 exchanges. The model is extended by accounting for scalar mesons, namely σ, $f_0(980)$ and $f_0(1370)$, contributing to the S-wave behavior, as well as the tensor meson $f_2(1270)$ corresponding to the D-wave contributions, while also considering non-resonant P- and S-wave components. The model contains a number of free parameters, which are constrained from a global fit of the available experimental data for angular moments up to $L = 2$ for $M = 0, ..., 2$. The fitted angular moments are compared with experimental data obtained from CLAS. The key physical insights gained from the model are summarized. Furthermore, we extract the t-dependence of the Regge amplitude residue function for the subdominant exchanges, shedding light on their contribution to the overall dynamics.

1 Introduction

The study of hadronic photoproduction stands as a vital method for gaining insights into the spectroscopic and structural properties of hadrons. Employing protons as targets enables researchers to probe the spectrum of excited nucleons at low energies. At higher energies, the dominance of t-channel Reggeon exchanges, as predicted by Regge theory, offers an opportunity to explore the process and extract information about the exchanged Reggeons.

*e-mail: nadine.hammoud.28@gmail.com

This proceedings focuses on providing a theoretical description of two (charged) pion photoproduction in the low invariant mass range of the $\pi\pi$ system [1]. In this kinematic region, a distinct peak that may be attributed to the presence of the $\rho(770)$ resonance. In addition to this dominant resonance, several other contributions, including S-wave resonances ($\sigma/f_0(500)$, $f_0(980)$, $f_0(1370)$) and the D-wave resonance $f_2(1270)$, are anticipated to affect the cross section. Furthermore, it is anticipated that forthcoming data releases from both CLAS12 and GlueX will provide additional insights into this process.

The proceedings are organized into sections detailing the kinematics of the process (Sec.2), an exploration of the model components (Sec.3), and predictions regarding angular moments (Sec.4).

2 Kinematics

In these proceedings, we describe a theoretical model for the process

$$\vec{\gamma}(q,\lambda_\gamma) + p(p_1,\lambda_1) \to \pi^+(k_1) + \pi^-(k_2) + p(p_2,\lambda_2)\,,$$

within the $\pi^+\pi^-$ helicity rest frame, where the $\pi^+\pi^-$ system remains stationary ($\mathbf{k}_1 = -\mathbf{k}_2$), and the recoiling proton ($\mathbf{p}_2$) is set as the negative z-axis. The reaction plane, involving the photon, target, and recoiling proton, defines the x-y plane, while the perpendicular axis becomes the y-axis. Here, $\Omega^{\rm H} = (\theta^{\rm H}, \phi^{\rm H})$ describes the π^+ angles relative to the z-axis.

The scalar amplitudes in this $2 \to 3$ process are defined by five independent kinematic variables: two angles for the π^+ and the invariants s, t, and $s_{\pi\pi}$.

$$s = (p_1+q)^2 = (p_2+k_1+k_2)^2\,, \tag{1}$$
$$t = (p_1-p_2)^2 = (k_1+k_2-q)^2\,, \tag{2}$$
$$s_{\pi\pi} = (k_1+k_2)^2 = (p_1-p_2+q)^2 = m^2_{\pi\pi}\,, \tag{3}$$
$$u_i = (q-k_i)^2\,; \quad i = 1,2. \tag{4}$$

The phase-space and intensity conventions are referenced from Ref. [2]. This work centers on computing angular moments, obtained as integral moments of the cross-section:

$$\langle Y_{LM}\rangle(s,t,m_{\pi\pi}) = \sqrt{4\pi}\int d\Omega\,\frac{d\sigma}{dt dm_{\pi\pi} d\Omega^{\rm H}}\,{\rm Re}\,Y_{LM}(\Omega^{\rm H})\,.$$

3 Model Description

The process of double pion photoproduction can be described as being due to the interplay of two fundamental processes, depicted in Figure 1. The Deck contribution [1a,1b] originates from complementary processes involved in the diffractive dissociation of the photon from the nucleon target. These processes predominantly stem from long-range interactions, prominently featuring one-pion exchange. Factorizing the one-pion exchange (as depicted in Fig. [1]), reveals a $2 \to 2$ subprocess related to elastic πN scattering. Within this model, the resonant peak at $m_{\pi\pi} \sim 0.8$ GeV is attributed to the production of the $\rho(770)$ resonance. Furthermore, the Particle Data Group (PDG) catalog encompasses various resonances below and above 1 GeV, each expected to contribute significantly to this process. Incorporating each of these resonances involves postulating a Regge production amplitude, a topic which will be elaborated upon in the subsequent sections.

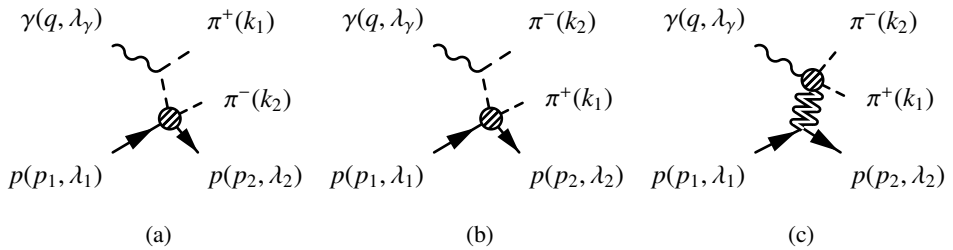

Figure 1: Key contributions to two-pion photoproduction: Deck topology in Figures [1a] and [1b], and resonant contribution in Figure [1c].

3.1 Resonance Model

In this approach, the resonances at the upper vertex are characterized as a product of production and decay amplitudes, shaped by a Breit-Wigner distribution i.e. BW:

$$\mathcal{M}_{\lambda_1\lambda_2\lambda_\gamma}(s,t,s_{\pi\pi},\Omega^{\mathrm{H}}) = BW(s_{\pi\pi})\sum_{\lambda_R}\mathcal{M}^{\gamma N\to RN}_{\lambda_1\lambda_2\lambda_\gamma\lambda_R}\Gamma^{R\to\pi\pi}_{\lambda_R}\,, \tag{5}$$

The model includes significant light meson resonances: $f_0(500)/\sigma$, $\rho(770)$, $f_0(980)$ below 1 GeV, and $f_2(1270)$ and $f_0(1370)$ above 1 GeV. In the CLAS kinematic range, the quasi $2\to 2$ process may be expressed as a sum of t-channel Reggeon exchanges, E. According to Regge theory, the amplitude factorizes into a Regge propagator, $R^E(s,t)$, and two vertices, T^E and B^E, functions of the momentum transfer. Hence,

$$\mathcal{M}^{\gamma N\to RN}_{\lambda_1\lambda_2\lambda_\gamma\lambda_R}(s,t,s_{\pi\pi}) = \sum_E T^E_{\lambda_\gamma\lambda_R}(t;s_{\pi\pi})R^E(s,t)B^E_{\lambda_1\lambda_2}(t)\,. \tag{6}$$

The Regge propagator structure depends on the nature of the exchanged Reggeon:

$$R^E(s,t) = \begin{cases} \dfrac{1+e^{-i\pi\alpha^E(t)}}{\sin\pi\alpha^E(t)}\left(\dfrac{s}{s_0}\right)^{\alpha^E(t)}, & E=\pi,\eta,\ \text{(unnatural)}\,,\\[2ex] \dfrac{\alpha^E(t)}{\alpha^E(0)}\dfrac{1+e^{-i\pi\alpha^E(t)}}{\sin\pi\alpha^E(t)}\left(\dfrac{s}{s_0}\right)^{\alpha^E(t)}, & E=\mathbb{P},f_2,a_2\ \text{(natural)}\,, \end{cases} \tag{7}$$

Here, $\alpha^E(t) = \alpha^E_0 + \alpha^E_1 t$ signifies the Regge trajectory, and $s_0 = 1$ GeV^2 denotes a fixed mass-scale. The t-dependence of vertices is not determined by Regge theory; it requires data inference or model assumptions. In this case, a Regge model is aligned with a one-particle exchange model, establishing the forms of $T_{\lambda_\gamma\lambda_R}(t;s_{\pi\pi})$, $B_{\lambda_1\lambda_2}(t)$, and $\Gamma^{R\to\pi\pi}_{\lambda_R}$ vertices. The P-wave amplitude can be found in Ref. [3]. Flexibility is maintained by partial wave projecting each resonant amplitude and weighting them with a complex free parameter g_{LM}. These parameters are adjusted to fit experimental data.

3.2 Background Model

3.2.1 Deck Mechanism

The Deck Mechanism unfolds as a sequential process, where a single off-shell pion, arising from photon decay, elastically recoils against the nucleon target, leading to the final state

$p\pi^+\pi^-$. The gauge-invariant Deck Model's amplitude, as formulated in [4–8], is expressed as:

$$\mathcal{M}^{\text{GI Deck}}_{\lambda_1\lambda_2\lambda_\gamma}(s,t,s_{\pi\pi},\Omega) = \sqrt{4\pi\alpha}\Big[\Big(\frac{\epsilon(q,\lambda_\gamma)\cdot k_1}{q\cdot k_1} - \frac{\epsilon(q,\lambda_\gamma)\cdot(p_1+p_2)}{q\cdot(p_1+p_2)}\Big)\beta(u_1)M^-_{\lambda_1\lambda_2}(s_2,t;u_1) - \Big(\frac{\epsilon(q,\lambda_\gamma)\cdot k_2}{q\cdot k_2} - \frac{\epsilon(q,\lambda_\gamma)\cdot(p_1+p_2)}{q\cdot(p_1+p_2)}\Big)\beta(u_2)M^+_{\lambda_1\lambda_2}(s_1,t;u_2)\Big], \tag{8}$$

The term $\beta(u_i) = \exp\Big((u_i - u_i^{\min})/\Lambda_\pi^2\Big)$ acts as a form factor suppressing the pion propagator for one-pion exchange at large u_i, where $\Lambda_\pi = 0.9$ GeV. $M^\pm_{\lambda_1\lambda_2}$ symbolizes the scattering amplitudes for $p + \pi^{*\pm} \to p + \pi^\pm$. The pursuit of gauge invariance includes a phenomenological contact term V^μ [9]. Despite being a binary amplitude, its reliance on three kinematic invariants arises from the initial pion's virtuality, u_i. As $u_i \to m_\pi^2$, these amplitudes are related to elastic $\pi^\pm p$ scattering, about which much is known, both experimentally and theoretically.This study employs πN scattering amplitudes from Ref. [10], combining the SAID partial wave parameterization [11] at lower energies with a Regge description at higher center-of-mass energies.

3.2.2 S and P-Waves Non-Resonant Pieces

In exploring resonant and non-resonant contributions, unique characteristics emerge in cross-section data. Resonances often reveal distinct peaks tied to particular energies and decay widths. However, addressing non-resonant backgrounds, inclusive of both P- and S-wave components, introduces complexity. An adaptable method involves employing a simplified parameterization with minimal variables to effectively describe the intricate background behavior. This parameterization is represented by:

$$F_{bkg}(s_{\pi\pi}) \equiv [(s^{\text{th}}_{\pi\pi} - s_{\pi\pi})(s^{\max}_{\pi\pi} - s_{\pi\pi})]\,, \tag{9}$$

where

$$s^{\text{th}}_{\pi\pi} = 4m_\pi^2 \tag{10}$$

$$s^{\max}_{\pi\pi} = s + m_p^2 - \frac{1}{2m_p^2}\Big[(s+m_p^2)(2m_p^2 - t) - \lambda^{1/2}(s,m_p^2,0)\lambda^{1/2}(t,m_p^2,m_p^2)\Big]. \tag{11}$$

Consequently, expressing the non-resonant component within the P-wave contribution:

$$\mathcal{M}^{\text{nr}}_{\mathbf{P}} = R_{f_2}(s,t)\frac{1}{s}F_{bkg}(s_{\pi\pi})\overline{u}(p_2,\lambda_2)\psi'(\lambda_\gamma)u(p_1,\lambda_1)\,, \tag{12}$$

where the parameters related to the non-resonant P amplitude are denoted as $a^{\text{nr}}_+(t)$, $a^{\text{nr}}_-(t)$, and $a^{\text{nr}}_0(t)$. Similarly, the formulation of the non-resonant S-wave contribution can be expressed as:

$$\mathcal{M}^{\text{nr}}_{\mathbf{S}} = \frac{1}{s}(a^{\text{nr}}_{s_j} + ib^{\text{nr}}_{s_j})R(s,t)[(s^{\text{th}}_{\pi\pi} - s_{\pi\pi})(s^{\max}_{\pi\pi} - s_{\pi\pi})]\overline{u}(p_2,\lambda_2)\gamma^\mu u(p_1,\lambda_1)v_\mu(\lambda_\gamma)\,. \tag{13}$$

4 Results and Conclusion

A comprehensive analysis has been conducted for six angular moments ($\langle Y_{00}\rangle, \langle Y_{10}\rangle, \langle Y_{11}\rangle, \langle Y_{20}\rangle, \langle Y_{21}\rangle$, and $\langle Y_{22}\rangle$) across all t bins using statistical bootstrapping in the presented model. The fit results for these moments at the highest momentum

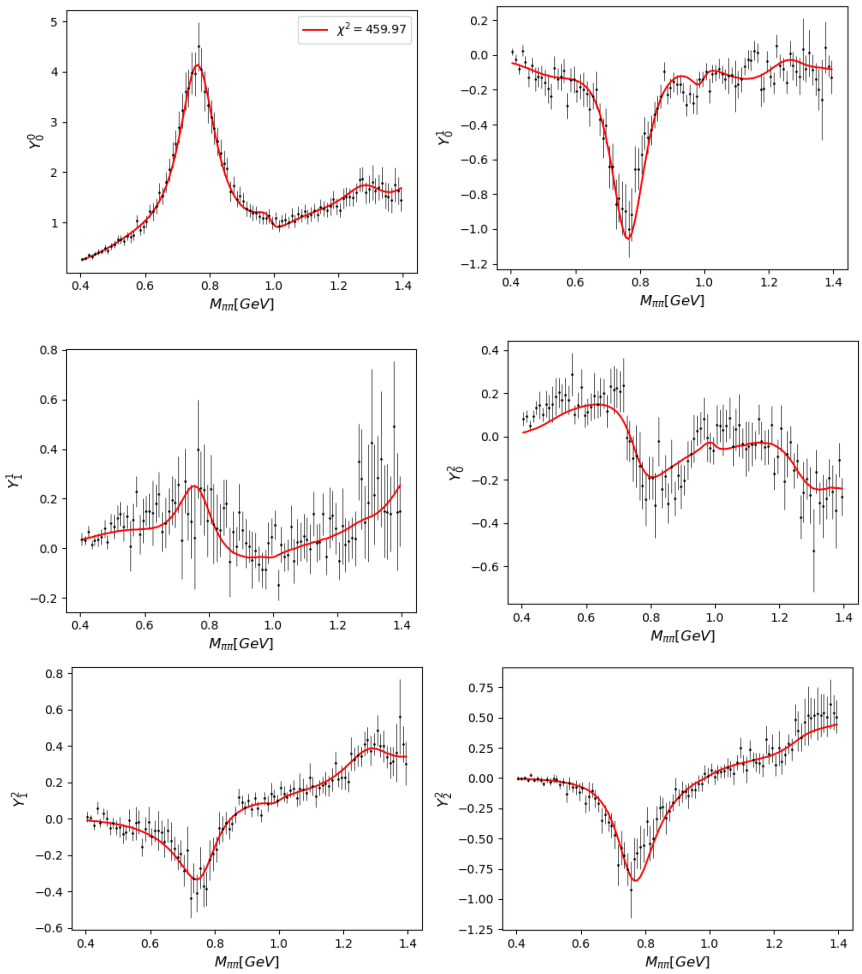

Figure 2: The fitted results of the angular moments (in red) vs. experimental results from CLAS [1] (in black) at $E_\gamma = 3.7$ GeV and $t = -0.95$ GeV^2.

transfer i.e. $t = -0.95$ GeV^2 are depicted in Figure 2. With a total of 30 free parameters, the model includes contributions from different resonances: 2 for scalar meson resonances in the S-wave as well as for the non-resonant piece, 6 for the ρ resonance in the P-wave and for the non-resonant piece, and 10 for the tensor meson f_2 in the D-wave. The agreement between the model and data highlights its capability in capturing crucial features of two-pion photoproduction within this kinematic region.

Analyzing the fits across all t bins reveals key insights:

- $\langle Y_{00} \rangle$: The dominant contributions to the differential cross-section arise from the $\rho(770)$ meson, followed by the tensor meson $f_2(1270)$. The scalar meson $f_0(980)$ exhibits a minimal impact, noticeable as a small bump.
- $\langle Y_{10} \rangle$ and $\langle Y_{11} \rangle$: In $\langle Y_{10} \rangle$, emergence of the S-wave contributions is observed, with dips indicating the $\rho(770)$ and scalar resonance σ. $\langle Y_{11} \rangle$ shows interference between the S- and

dominant P-waves, reflected in a bump at $m_{\pi\pi} \sim 0.77$ GeV due to this interplay and distinct peaks representing tensor and scalar resonances at $m_{\pi\pi} > 1.2$ GeV.

- $\langle Y_{20} \rangle$, $\langle Y_{21} \rangle$, and $\langle Y_{22} \rangle$: These moments demonstrate the interplay among P-wave contributions and other wave components. Scalar resonances might not be pronounced at low t, but they become more visible in $\langle Y_{21} \rangle$ and $\langle Y_{22} \rangle$ for $t = -0.55 \ \rightarrow -0.95$ GeV^2.

Prospective research avenues involve exploring the t-dependency of the g_{LM} parameters and extending the model's applicability to forecast outcomes for experiments like CLAS12 and GlueX, particularly at higher photon energies. Further investigation into the helicity structure and the amplitude's behavior concerning variable t presents promising opportunities for in-depth analysis.

The proceedings presented a theoretical model integrating various $\pi\pi$ resonances across S, P, and D waves, coupled with a key background contribution from the Deck mechanism in two-pion photoproduction. Successful alignment with experimental data was achieved by optimizing the relative weights of partial waves, underscoring the model's ability to accurately portray production mechanisms and critical partial waves that govern angular moments.

This model's potential extends to making predictions at photon energies relevant to CLAS12 and GlueX experiments, showcasing its utility in future experimental analyses and predictive capabilities.

Acknowledgements

This work was supported by Project No. 2018/29/B/ST2/02576 from the National Science Center in Poland. Additionally, we acknowledge the support of Project PID2020-118758GB-I00, funded by the Spanish MCIN/AEI/10.13039/501100011033/.

References

[1] M. Battaglieri et al. (CLAS), Phys. Rev. D **80**, 072005 (2009), 0907.1021
[2] V. Mathieu, M. Albaladejo, C. Fernández-Ramírez, A.W. Jackura, M. Mikhasenko, A. Pilloni, A.P. Szczepaniak (JPAC), Phys. Rev. D **100**, 054017 (2019), 1906.04841
[3] L. Lesniak, A.P. Szczepaniak, Acta Phys. Polon. B **34**, 3389 (2003), hep-ph/0304007
[4] L. Bibrzycki, P. Bydžovský, R. Kamiński, A.P. Szczepaniak, Phys. Lett. B **789**, 287 (2019), 1809.06123
[5] L. Bibrzycki, P. Bydžovský, R. Kamiński, A.P. Szczepaniak, EPJ Web Conf. **199**, 02009 (2019)
[6] L. Bibrzycki, P. Bydžovský, R. Kamiński, A.P. Szczepaniak, *Photoproduction of the S-, P- and D-wave resonances on protons in the $\pi^+\pi^-$ channel*, in *18th International Conference on Hadron Spectroscopy and Structure* (2020), pp. 410–415
[7] L. Bibrzycki, P. Bydžovský, R. Kamiński, A.P. Szczepaniak, Acta Phys. Polon. Supp. **13**, 77 (2020)
[8] N. Hammoud, PoS **ICHEP2022**, 837 (2022)
[9] J. Pumplin, Phys. Rev. D **2**, 1859 (1970)
[10] V. Mathieu, I.V. Danilkin, C. Fernández-Ramírez, M.R. Pennington, D. Schott, A.P. Szczepaniak, G. Fox, Phys. Rev. D **92**, 074004 (2015), 1506.01764
[11] R.L. Workman, R.A. Arndt, W.J. Briscoe, M.W. Paris, I.I. Strakovsky, Phys. Rev. C **86**, 035202 (2012), 1204.2277